Task-Level Control of the Lateral Leg Spring Model of Cockroach Locomotion

Jusuk Lee[1], Andrew Lamperski[2], John Schmitt[3], and Noah Cowan[1]

[1] Johns Hopkins University, Baltimore, MD, {jsl,ncowan}@jhu.edu
[2] California Institute of Technology, Pasadena, CA, andyl@cds.caltech.edu
[3] Oregon State University, Corvallis, OR, schmitjo@engr.orst.edu

Summary. The Lateral Leg Spring model (LLS) was developed by Schmitt and Holmes to model the horizontal-plane dynamics of a running cockroach. The model captures several salient features of real insect locomotion, and demonstrates that horizontal plane locomotion can be passively stabilized by a well-tuned mechanical system, thus requiring minimal neural reflexes. We propose two enhancements to the LLS model. First, we derive the dynamical equations for a more flexible placement of the center of pressure (COP), which enables the model to capture the phase relationship between the body orientation and center-of-mass (COM) heading in a simpler manner than previously possible. Second, we propose a reduced LLS "plant model" and biologically inspired control law that enables the model to follow along a virtual wall, much like antenna-based wall following in cockroaches.

Key words: spring-mass system, legged locomotion, return map

1 Introduction

For decades, researchers have posited low-dimensional spring-mass models to describe the COM dynamics and ground reaction forces in a broad variety of running animals [2, 4, 9, 11, 12, 19]. In order to understand the complex body mechanics of running animals, they have simplified the problem by decoupling the mechanics into the sagittal and horizontal planes. For animals whose locomotion occurs primarily in the sagittal plane, the locomotion dynamics have been modeled as a spring-loaded inverted pendulum (SLIP) [2, 16, 26, 27]. Insects, whose motion occurs primarily in the horizontal plane, have dynamics that have been approximated by a lateral leg spring (LLS) model [23, 24]. Results of the LLS suggest that the mechanical structure of an insect may be used to produce stable periodic gaits when running at high speeds, without relying solely on proprioceptive reflexes and detailed neural feedback for stability.

The LLS models insect locomotion, specifically that of the cockroach *Blaberus discoidalis*. Cockroaches run using an alternating tripod gait [4]. Experiments have shown that the forces produced by this tripod of legs can be well represented by a single effective leg [10, 15]. Since the total mass of the legs of the insect is less

than 6% of the total mass, the LLS model approximates each alternating tripod as a single massless, spring-loaded *virtual leg* that attaches to the midline of the body at a point called the center of pressure (COP). As illustrated in Fig. 1, the COP is offset from the center of mass (COM) by a displacement, d, where d may lie in front of the COM ($d > 0$) or behind the COM ($d < 0$). The model assumes that the foot pivots freely without slipping about its attachment to the ground, r_{foot}, and that the leg can rotate freely about the COP. This implies that no moments about the foot or COP can be generated, and forces will be applied to the body along the length of the leg. A full stride for the model consists of a left and right step phase. A step phase begins with the relaxed spring extended at an angle $\pm\beta_0$ with respect to the body centerline. The body moves forward, compressing and extending the elastic spring, until the spring returns to its original length, at which point the leg is lifted, the next leg is placed down, and the cycle repeats.

Changes in the foot placements between left and right step phases result in a hybrid dynamical system. Systems with piecewise-holonomic constraints such as these can display asymptotic stability [21]. For gaits encountered in the LLS model, periodic motions exhibit neutral eigendirections due to energy conservation and SE(2) invariance. Therefore, stability is partially asymptotic in the sense that perturbations to periodic orbits in the direction of the eigenvectors of conserved quantities and symmetries do not grow or decay, but simply result in movement to a different, stable gait. Gaits in the LLS model display partial asymptotic stability in the heading direction and angular velocity as a result of angular momentum trading between left and right step phases. The mechanical structure of the model therefore self-stabilizes the locomotion system [23]. If $d < 0$ then the gaits are asymptotically stable in heading and angular velocity, i.e. the body approaches straight trajectories if the trajectory begins in the basin of attraction for the stable periodic orbit. If $d = 0$, the periodic orbits exhibit neutral stability in angular velocity and asymptotic stability in heading. If $d > 0$, periodic orbits are unstable. To show stability, one takes Poincaré sections at the beginning of a full stride, and numerically approximates the fixed points and eigenvalues of the linearized return map.

While the energetically conservative fixed and moving center of pressure models of [23, 24] reproduce many salient features of the kinematics and forces exhibited experimentally by *Blaberus discoidalis*, detailed comparisons illuminate limitations of the LLS. In particular, the fixed COP models previously investigated consider only COPs on the fore-aft body axis, and consequently only produce sinusoidal variations in θ; in contrast, the animal produces cosinusoidal variations [28]. This is due to the fact that a fixed COP located behind the center of mass along the fore-aft body axis is only capable of producing a positive or negative moment, rather than a moment that changes sign during each step phase. Additionally, fore-aft and lateral force profile magnitudes are typically reversed in comparison to those observed experimentally. Allowing the leg attachment point to vary from fore to aft in the moving COP model serves to address the qualitative discrepancies in the moment and yawing profiles. However, while qualitatively correct yaw and moment profiles are produced by the model, quantitative comparisons reveal that the variations in each remain an order of magnitude smaller than those observed experimentally. An activated muscle model introduced by Schmitt and Holmes [25] attempts to correct the moment and yawing oscillations by introducing hip torques and muscle activation. While these authors obtained correct moment profiles in this manner, they are obtained at the expense of increased model complexity and inverted fore-aft force profiles.

The goal of this paper is to modify the LLS model to better match the actual cockroach, with as few parameters as possible, and to extend it to serve as a plant model for control. To compare our model to the previous LLS, we consider features salient to cockroach locomotion, such as stability, body motion kinematics, forces and moments, stride frequency, etc. For control, we use a biologically inspired antenna-like measurement [6–8], and show numerically that the closed-loop system dynamics asymptotically track a virtual wall in the environment. In addition, the controller maintains the LLS model's energy conserving nature.

2 Dynamics and Simulation of an Enhanced LLS Model

The goal of this research is to control the LLS model from step-to-step to achieve a locomotion objective such as following along a wall and avoiding obstacles in a planar environment. Using a controlled form of the LLS as a "plant model" may provide insights into our longer term objective of controlling a legged robot such as RHex [1], Sprawl [5], or Whegs [20]. It is known, for example, that RHex exhibits a dynamically similar gait in both the sagittal and horizontal planes to a cockroach. Toward that end, this section explores the effects of COP placement and movement on the steady-state dynamics of the LLS model. The goal is to uncover the simplest possible mechanism to match biological data, while still providing the possibility for control.

2.1 LLS Dynamics with 2-D COP Placement for a Left Step

We propose an alternative (or a simpler) solution to the moving COP; laterally offset the fixed COP (i.e. position the COP in the positive x-direction of the body frame $\{B\}$). This has a similar effect as the moving COP scheme; the leg generates a clockwise torque during the first half of a step, and an opposite torque during the last half, assuming the body angle, θ, is greater than zero at the start of a left-leg step.

In order to validate our alternative solution, we represent the position of the COP during the left-leg step as:

$$\begin{bmatrix} d_1 \\ d_2 \end{bmatrix} = \begin{bmatrix} b_1 + c_1(\psi - \theta) \\ b_2 + c_2(\psi - \theta) \end{bmatrix}, \tag{1}$$

where d_1 and d_2 are along the x and y-axis of the LLS body frame $\{B\}$, and ψ and θ are shown in Fig. 1. In this representation, we allow the COP to be either fixed ($c_1 = c_2 = 0$) or moving ($c_1 \neq 0$ or $c_2 \neq 0$) from any offset (b_1 and b_2) in the body frame $\{B\}$. This freedom allows us to test different COP placement protocols, including the case where the COP moves backwards while offset to the side [28]. This representation implicitly assumes that during the next right-leg step, the COP position will be mirrored about the y-axis about the body frame $\{B\}$. If $d_1 = 0$, then we have the equation introduced in [23].

Consider the generalized coordinates $r = (\zeta, \psi, \theta)$, as depicted in Fig. 1. For the left step phase, the Hamiltonian of the LLS system implemented with a linear spring is

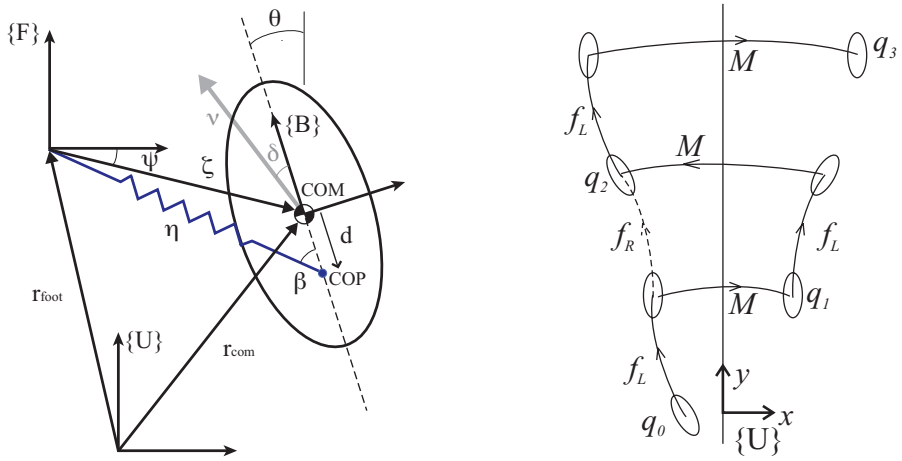

Fig. 1. *Left:* A schematic model of the LLS model, showing the coordinates used for expressing Hamilton's equations. *Right:* Illustration of multi-step dynamics. The dynamics of each left step phase are given by (4). A right step can be achieved by first flipping the states about the y-axis, integrating the left step map, and then flipping back. Breaking this chain in the correct place leads to a single "integrate and flip" return map, $f(q) := Mf_L(q)$, that will simplify controller design.

$$H = \frac{p_\zeta^2}{2m} + \frac{p_\psi^2}{2m\zeta^2} + \frac{p_\theta^2}{2I} + \frac{k(\eta - l_0)^2}{2} \tag{2}$$

where ζ, ψ, k, l_0, I, and m denote the distance from the foot placement to the COM, the angle from the foot placement to the COM, the linear spring stiffness, the relaxed leg length, the moment of inertia, and the mass, respectively. The length of the leg is given in terms of the COP location by

$$\eta = \Big[b_1^2 + b_2^2 + \zeta^2 + \phi\big(2b_1c_1 + 2b_2c_2 + (c_1^2 + c_2^2)\phi\big) + 2\zeta\big((b_1 + c_1\phi)\cos\phi + (b_2 + c_2\phi)\sin\phi\big)\Big]^{1/2}. \tag{3}$$

Hamilton's equations of motion with our new COP and the linear leg spring model are given by

$$\begin{aligned}
\dot\zeta &= \frac{p_\zeta}{m}, \qquad \dot p_\zeta = \frac{p_\psi^2}{m\zeta^3} - \frac{k(\eta - l_0)}{\eta}\big(\zeta + (b_1 + c_1\phi)\cos\phi + (b_2 + c_2\phi)\sin\phi\big),\\
\dot\psi &= \frac{p_\psi}{m\zeta^2}, \quad \dot p_\psi = -\frac{k(\eta - l_0)}{\eta}\big(b_1c_1 + b_2c_2 + (c_1^2 + c_2^2)\phi\\
&\qquad\qquad + \zeta(b_2 + c_1 + c_2\phi)\cos\phi - \zeta(b_1 - c_2 + c_1\phi)\sin\phi\big),\\
\dot\theta &= \frac{p_\theta}{I}, \qquad \dot p_\theta = -\dot p_\psi,
\end{aligned} \tag{4}$$

where $\phi \triangleq \psi - \theta$. We assume when a step commences, the spring is uncompressed, $\eta = l_0$. Because the spring starts at and returns to rest length at step transitions, no step-to-step impacts dissipate energy, and thus energy is conserved in the LLS model.

2.2 Hybrid Step-to-Step Dynamics

The generalized coordinates $r = (\zeta, \psi, \theta)$ and their conjugate momenta, p_r, provide a convenient set of local coordinates for expressing the *within-step* Hamiltonian dynamics (4) of the LLS. However, they provide an inconvenient representation when considering the *step-to-step* dynamics because they depend on the frame $\{F\}$ that moves every step. As a remedy, we follow [23], and use $q = (s, g) \in \mathcal{S} \times \mathrm{SE}(2)$, where $s = (v, \delta, \dot{\theta}) \in \mathcal{S} \subset \mathbb{R}^3$ are the "internal" states, and $g \in \mathrm{SE}(2)$ is the pose. The speed, v, is the magnitude of the COM velocity, and the relative heading, δ, is the angular difference between the orientation, θ, and the angle of the COM velocity vector (see Fig. 1). The local coordinates (θ, x, y) parameterize SE(2) without singularities through the usual relationship,

$$g = \begin{bmatrix} \cos\theta & -\sin\theta & x \\ \sin\theta & \cos\theta & y \\ 0 & 0 & 1 \end{bmatrix} \tag{5}$$

(written as a homogeneous transformation matrix) so we conflate the two when convenient and often write $g = (\theta, x, y)$ in an abuse of notation. The dynamical equations can be recast using the state variables q, which we omit for simplicity of presentation. Instead, we consider the state q_i, $i = 0, 1, 2 \ldots$ as the discrete state, where $q_k = (s_k, g_k)$ corresponds to the state at the beginning of the k^{th} step. If $h \in \mathrm{SE}(2)$ and $q = (s, g) \in \mathcal{S} \times \mathrm{SE}(2)$ then we define the left action of SE(2) on $\mathcal{S} \times \mathrm{SE}(2)$ by $hq = (s, hg)$, where hg is the group product on SE(2).

At the beginning of the k^{th} step (for k even), the leg is at rest length, $\eta = l_0$, and the leg touch-down angle starts at β_0 relative to the y-axis of the body frame $\{B\}$, $\beta = \beta_0$. This information, together with the state $q_k = (s_k, g_k)$, uniquely determines the initial conditions for integration of Hamilton's equations. When η again reaches the spring rest length l_0, the hybrid system transitions to the right step, as described below. The final values of (r, p_r) at the end of the k^{th} step uniquely determine the states $q_{k+1} = (s_{k+1}, g_{k+1})$, used to start the subsequent step. Thus, the left step dynamics map the state $f_L : q_k \mapsto q_{k+1}$ according to a simple change of variables into coordinates (r, p_r), followed by integration of Hamilton's equations. By inspection of Hamilton's equations (4), note that the left-step mapping is left invariant under rigid transformations of the initial condition, since the equations are not functions of (x, y), and θ never shows up without $-\psi$, both of which are with respect to the world frame. Hence, $f_L(s, hg) = h f_L(s, g)$. Note that this implies that $q_{k+1} = (s_{k+1}, g_{k+1}) = f_L(s, g_k) = g_k f_L(s, e)$, where $e \in \mathrm{SE}(2)$ is the identity.

Let $\{A_k\}$ denote the location of the body frame at the beginning of the k^{th} step. In other words, g_k is the transformation from $\{A_k\}$ to the world frame $\{U\}$. For k odd, the right leg is down, and Hamilton's equations (4) are identical, so long as we express them in terms of a *left-handed* frame. We do this by taking a mirror image around the y-axis of frame $\{A_k\}$ at the beginning and end of the k^{th} step (k odd), to write down the right step map in terms of the left one. This can be expressed in terms of local coordinates $q = (v, \delta, \dot{\theta}, \theta, x, y)^T$ as first "flipping" $(\delta, \dot{\theta}, \theta, x)$, integrating the left step map, and then flipping back, namely

$$f_R(q) = M f_L\big(Mq\big), \text{ where } M = \mathrm{diag}\,\{1, -1, -1, -1, -1, 1\}\,. \tag{6}$$

Note that $MM = I$. We chose to flip about the y-axis for notational simplicity, but in principle any left-handed frame would work. This mapping leaves the right step map left-invariant under SE(2).

For finding symmetric steady-state gaits, it will be convenient to define a special step-to-step return map that amounts to an "integrate and flip" (see Fig. 1, *Right*). For a complete stride that includes a left step and then a right step, the stride-to-stride mapping is given by $f_{L-R} = f_R \circ f_L$, namely

$$f_{L-R} : q \mapsto Mf_L(Mf_L(q)) = (f \circ f)(q), \quad \text{where} \quad f(q) := Mf_L(q). \tag{7}$$

This approach eliminates the need to distinguish between left and right steps for control purposes. Note, however, that f is *not* left-invariant, even though both f_L and f_R are left-invariant. The resulting state evolution is given simply by

$$q_{k+1} = f(q_k), \tag{8}$$

keeping in mind that for odd steps, the value for q_k in this step-to-step formulation has already been "flipped".

2.3 Simulation Methods

We simulated the LLS model using Matlab and the convention discussed in Sect. 2.2; for every right-step, convert it to a left-leg step, simulate the within step dynamics, and then convert it back to a right-leg step. This enabled us to specify the COP position using (1) and integrate the equation of motion (4) without the explicit representations of a left or right step in the equations. We used Matlab's `ode45` with time varying step size to integrate the equations of motion. The integration terminated as soon as the compressed leg returned back to its relaxed length l_0. To specify a moving COP, we selected b_i and $d_i(kT)$, $i = 1, 2$ where $d_i(kT)$ denotes the COP position at the start of k-th step. To meet this restriction, c_i is allowed to vary at each step, although it shouldn't vary at an equilibrium point.[4]

We found the equilibrium point $q_0 = (v, \delta, \theta, \dot{\theta}, x)^T$ using the Levenberg-Marquardt method in Matlab's `fsolve` function. While fixing the state v to a desired value, the function minimized the error difference of a step, $f(q) - q$. We also found the stride-to-stride Jacobian, A_{stride}, and step-to-step Jacobian, A_{step}, about the equilibrium point using a central difference approximation. The i^{th} columns are given by $[A_{\text{stride}}]_i = (f_{L-R}(q + e_i\epsilon) - f_{L-R}(q - e_i\epsilon))/2\epsilon$ and $[A_{\text{step}}]_i = (f(q + e_i\epsilon) - f(q - e_i\epsilon))/2\epsilon$, where $\epsilon = 1 \times 10^{-6}$ and e_i is the i-th column of 5×5 identity matrix. In Sect. 3.2, we discuss the LLS stability from the eigenvalues of A_{stride}, while in Sect. 4, we use A_{step} to control the LLS model.

Unless otherwise noted, we used the following parameters and measurements of death-head cockroaches, *Blaberus discoidalis,* used in [19,22,24]: $m = 0.0025\,\text{kg}$, $I = 2.04 \times 10^{-7}\,\text{kg}\,\text{m}^2$. The choices for l_0, k, v, and β_0 were chosen to satisfy constraints on the stride length ($L_s = 0.02 - 0.025\,\text{m}$) and stride frequency ($f_s = 10\,\text{Hz}$), and generally fell in the ranges $k = 2.25 - 3.5\,\text{N}\,\text{m}^{-1}$, $l_0 = 0.008 - 0.015\,\text{m}$, $\beta_0 = 0.8 - 1.2\,\text{rad}$, $d_i = 0.002\,\text{m}$, and $v = 0.2 - 0.25\,\text{m/s}$.

[4] Instead, the values for b_i and c_i can be specified directly [24]. This causes $d_i(kT)$ to change depending on the quantity $(\psi(kT) - \theta(kT))$.

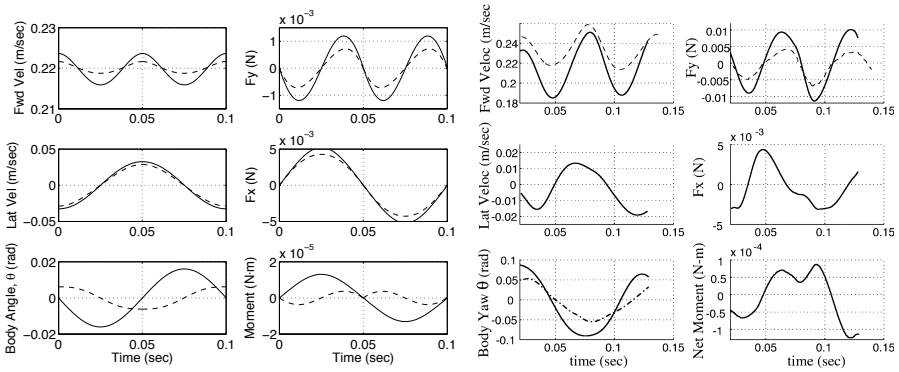

Fig. 2. *Left:* A stride of the original LLS model ($d_1 \equiv 0$) with a fixed COP (solid) and a moving COP (dashed). The used parameters for the fixed COP are: $v = 0.226$ cm/s, $k = 2.4$ N/m, $\beta_0 = 1$ rad, $l_0 = 0.0102$ m, $d_2 = -0.0025$ m; for the moving COP are: $v = 0.2235$ m/s, $k = 3.52$ N/m, $\beta_0 = 1.125$ rad, $l_0 = 0.0082$ m, $d_2 = 0.0025$ m $\rightarrow -0.0025$ m. *Right:* Experimental measurements of *Blaberus discoidalis* from several sources, [14, 15, 18]; figure from [22]. (Notice, since the right figure doesn't start from $t = 0$, the stride period is roughly the same between the two figures.)

3 Analysis of COP Placements

3.1 Effects of various COP placements

In order to match the LLS system with an actual cockroach data (Fig. 2), we need to understand the effects of b_i and c_i (or $d_i(kT)$) on the overall system. To do so, our initial attempt is to consider various protocols for the COP placements:

(a) Increment d_1 while $d_2 = 0$;
(b) Increment d_2 while $d_1 = 0$;
(c) Increment the amplitude of a moving d_2 while $d_1 = 0$;
(d) Increment the offset of a moving d_2 while $d_1 = 0$;
(e) Increment d_1 while d_2 is moving;

Figure 3 illustrates these protocols schematically for a left step; for a right step, the COP path is mirrored about the body y-axis. For each protocol and their parameter increments, we found the corresponding equilibrium points and simulated a full stride (starting with a left step) from the equilibrium points. The results from the simulations are shown in Figs. 4, 5, and 6. For each incrementing parameter, we plotted the result using different shades of gray. The first two columns of a subfigure shows the COM velocity and leg-spring forces in lateral and forward directions (i.e. x and y directions in the inertial frame $\{U\}$), the body angle, and the moment. The last column shows d_1 (solid line) and/or d_2 (dashed line) as a function of time, COM path, and the eigenvalues as a function of the incrementing parameter. The rest of the parameters (i.e. k, v, β_0, and l_0) were chosen to closely match the stride length and frequency of cockroach data [22].

Protocol (a): Fixed COP on lateral axis. Figure 4(a) shows results of a simulated LLS model in which we fixed the COP at various positions along the x-axis of

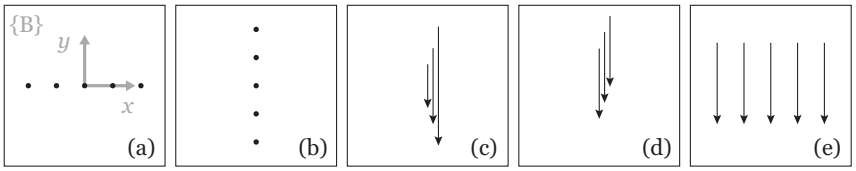

Fig. 3. COP placement protocols for a left step with respect to the body frame $\{B\}$. The solid dots indicate fixed COP positions; the arrows indicate the direction, magnitude, and offset of moving COPs.

the body frame $\{B\}$. As desired, when $d_1 > 0$, the profiles of the body angle, θ, and the moment waveforms resemble actual cockroach data (Fig. 2), as well as that of the moving COP proposed by Schmitt and Holmes [24] (reproduced in Fig. 2, *Left*). Note that the positive cosinusoidal waveforms of the body angle (which agrees with the biological data) for a fixed COP only occur when d is on the positive x-axis of $\{B\}$. Fig. 4(a) indicates that the increase in $|d_1|$ amplifies the body angle and the moment waveforms while the other measurements, including the stride length and frequency, remain relatively constant. This isolated effect of d_1 will be useful later on when we fit the data to another waveform. In addition, the eigenvalue plot shows that the system becomes unstable when $d_1 < 0$ and stable when $d_1 > 0$.

Protocol (b): Fixed COP on fore-aft axis. As a comparison to the previous result, Fig. 4(b) shows the effects of different locations d_2 for a fixed COP. Although the body angle is sinusoidal (not cosinusoidal, like the cockroach), the location of d_2 does have a larger impact on the magnitude of body angle and the stability of the system (steeper slope for the moving eigenvalue) than d_1 in the previous protocol. We speculate that one cause of this differences in impact level is due to the large value of β_0; since $\beta_0 = 1.12 > \pi/4$, the leg force is oriented primarily in the lateral direction rather than the fore-aft direction. Thus, changes in d_2 cause greater moment arm changes than the equal changes in d_1. We will utilize this effect in Sect. 4 by using d_2 as our control input. We also note that the body velocity (and position) and foot forces of this figure matches the previous figure. Although not shown, as the fixed COP position traverses in this neighborhood, without the restriction of $d_1 = 0$ or $d_2 = 0$, the body velocity and foot force waveforms remain relatively constant. On the other hand, the waveforms for the body angle and the moment go through phase and amplitude changes.

Protocol (c): Incrementing magnitude of a moving COP on the fore-aft axis. For fore-aft COP motion along the body frame y-axis, Fig. 5(c) shows the effects of changing the magnitude of COP motion. Unlike the previous protocols, varying the magnitude of a moving COP causes large changes to all the kinematics, step length, and step frequency. Although it is not shown here, further increase in magnitude (also observed in [22]) or reversing the direction (i.e. aft to fore) of the moving COP drives the system unstable.

Protocol (d): Forward Shifting of a Moving COP. Figure 5(d) shows the effects of shifting a moving COP in y direction in $\{B\}$. It shows that, as the offset b_2 increases (or decreases, although not shown), the body loses its cosinusoidal waveform and eventually becomes unstable. We emphasize that the system does not go unstable as soon as the offset $b_2 > 0$ nor $b_2 < 0$. Also the instability does not necessarily occur even though the moving COP remains in front of the COM most of the time.

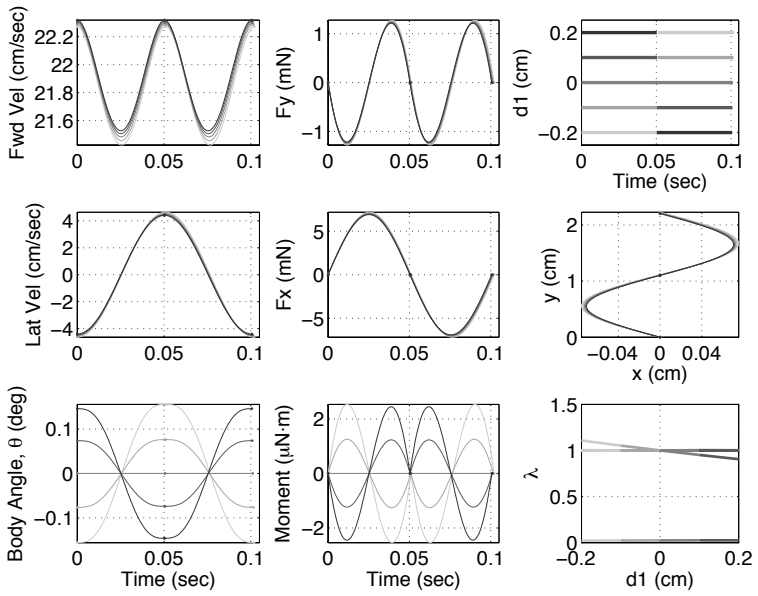

(a) Increment $d_1 = \{-0.2, \ldots, 0.2 \text{ cm}\}$ while $d_2 = 0$.

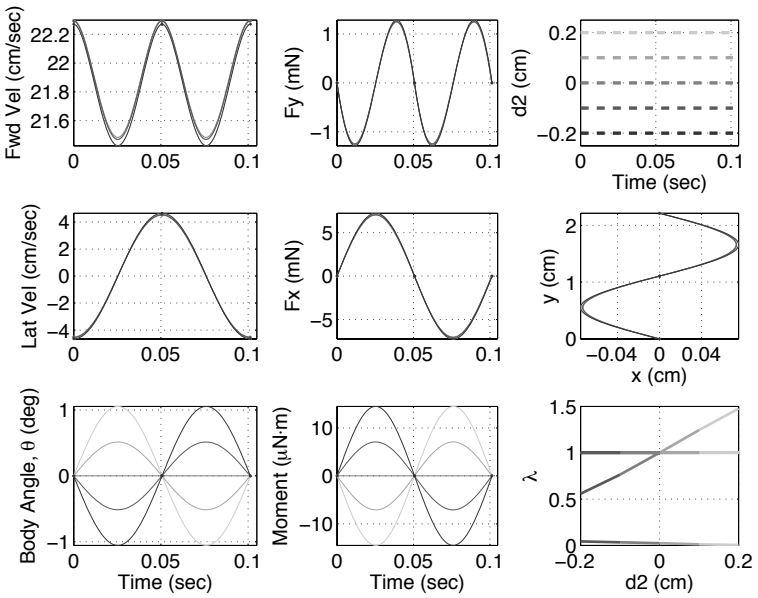

(b) Increment $d_2 = \{-0.2, \ldots, 0.2 \text{ cm}\}$ while $d_1 = 0$.

Fig. 4. See text for description of each COP protocol. The parameters used in this figure are: $m = 0.0025\,\text{kg}$, $I = 2.04 \times 10^{-7}\,\text{kg}\,\text{m}^2$, $k = 3.52\,\text{N}\,\text{m}^{-1}$, $v = 0.2275\,\text{m/s}$, $l_0 = 0.0127\,\text{m}$, $\beta_0 = 1.12\,\text{rad}$ (or 64.2°). Note, unlike Fig. 2, these figures have scaled units (e.g. cm and mN) for clarity.

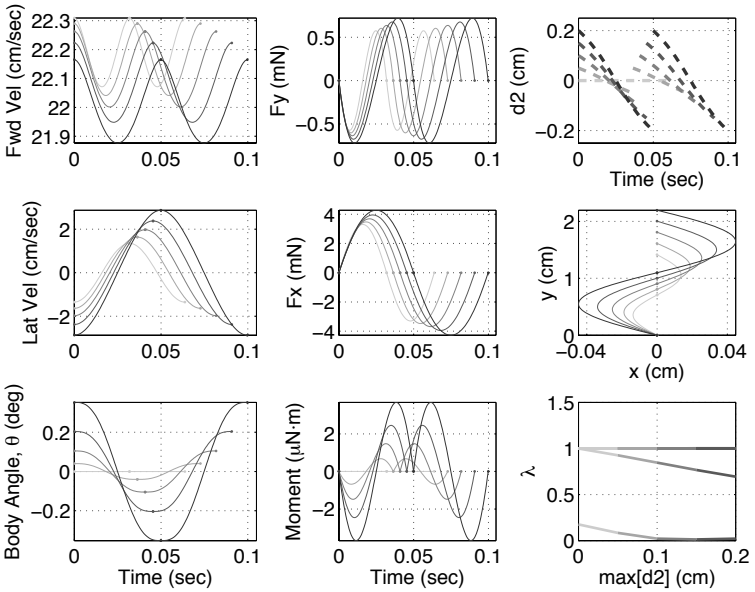

(c) Increment the amplitude of moving d_2 from 0 to 0.2 cm while $d_1 = 0$.

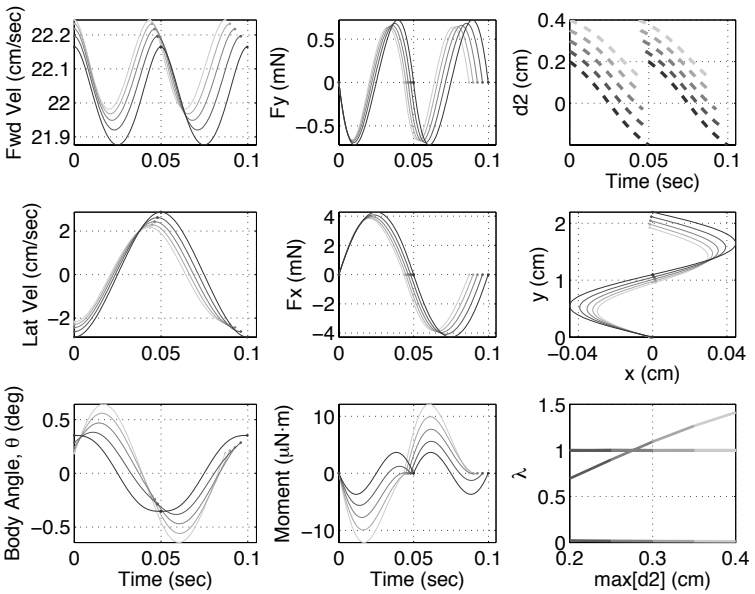

(d) Increment the offset of moving d_2 from 0 to 0.2 cm while $d_1 = 0$.

Fig. 5. The parameters used here are: $m = 0.0025\,\mathrm{kg}$, $I = 2.04 \times 10^{-7}\,\mathrm{kg\,m^2}$, $k = 3.52\,\mathrm{N\,m^{-1}}$, $v = 0.2235\,\mathrm{m/s}$, $l_0 = 0.0082\,\mathrm{m}$, $\beta_0 = 1.125\,\mathrm{rad}$.

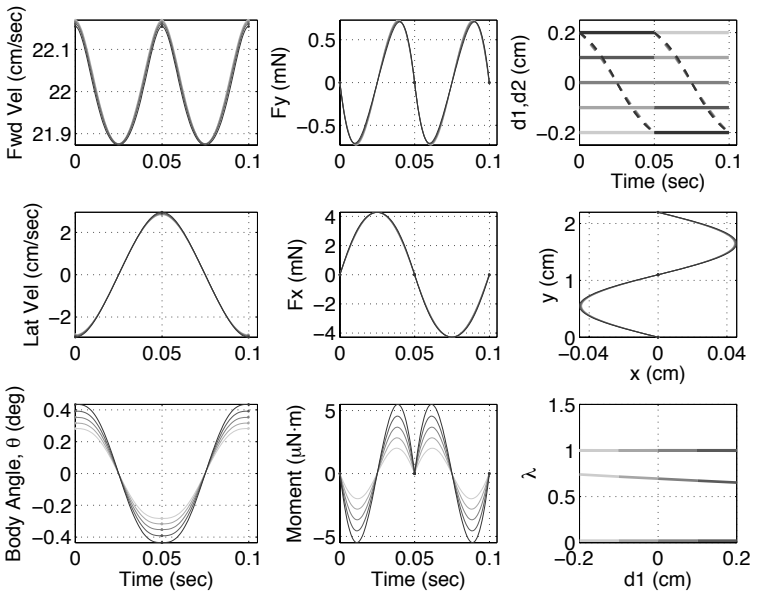

(e) Increment $d_1 = \{-0.2, \ldots, 0.2 \text{ cm}\}$ (solid) while d_2 (dashed) is moving from 0.2 to -0.2 cm.

Fig. 6. Parameters used are: $m = 0.0025$ kg, $I = 2.04 \times 10^{-7}$ kg m^2, $k = 3.52$ N/m, $v = 0.2235$ m/s, $l_0 = 0.0082$ m, $\beta_0 = 1.125$ rad.

Along with Protocol (c), we introduce one possible explanation of these results in Sect. 3.3.

Protocol (e): Lateral Shifting of a Moving COP. Lastly, we look at the result of incrementing the lateral offset to a moving COP, as shown in Fig. 6(e). The result resembles that of Protocol (a) in Fig. 4(a); the changes in d_1 mostly affect the magnitude of body angle and moments, but the waveforms all remain qualitatively the same shape. Also, the increase in d_1 has amplified the waveforms, and the moving COP has stabilized the system even with $d_1 < 0$, in contrast to the results of Fig. 4(a).

From the results from these protocols, we conclude that we can achieve the desired cosinusoidal waveforms by laterally offsetting a fixed COP or moving COP. However, both cases produce body angle and moment variations that remain an order of magnitude smaller than those of a cockroach. This can be remedied with a very large – possibly non-physical – COP offset of $d_1 = 0.025$ m $\approx 2l_0$ and $d_2 = 0$, which means that the virtual foot touchdown position will be far off to the positive x-axis in $\{B\}$ along with the COP. The resulting magnitude of the body angle was about 2° (or 0.035 rad) with the moment of 0.3×10^{-4} N m. This is within an order of magnitude of the cockroach variations 5.7° (or 0.1 rad) and 1×10^{-4} N m in Fig. 2.

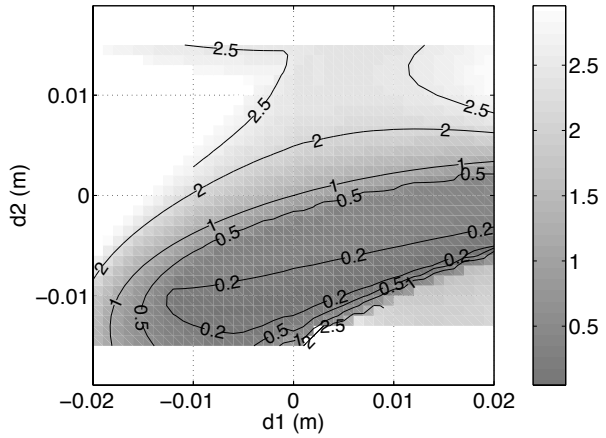

Fig. 7. Maximum eigenvalue (neglecting two invariant unity eigenvalues for energy and direction) of the linearized return map as a function of our new, two dimensional COP locations. The dark gray indicates the parameter regime of maximum stability and the neutral stability occurs when the contour reads 1. Eigenvalues greater that 3 are empty. The parameter values used are: $v = 0.25\,\mathrm{m/s}$, $k = 2.4\,\mathrm{Nm}^{-1}$, $l_0 = 0.01\,\mathrm{m}$, $\beta_0 = 1\,\mathrm{rad}$, and $-0.02\ \mathrm{m} < d_1, d_2 < 0.02\ \mathrm{m}$.

3.2 Stability as a Function of Fixed COP Position

Figures 4(a) and 4(b) showed the stability plot of the LLS with a fixed COP along the x and y-axis of $\{B\}$, respectively. Figure 7 shows a contour plot of the maximum non-unity eigenvalues as a function of more general 2D fixed COP positions. Note that the neutrally stable (i.e. $\max\lambda = 1$) gait corresponding to $(d_1, d_2) = (0, 0)$ found by Schmitt and Holmes [23] lies along a neutral stability contour through the origin of the d-plane. There is a large stable region ($\max\lambda < 1$) "inside" the neutral stability contour and an abrupt area of instability in the lower-right corner of the plot. Notice that the stable region ($\max\lambda < 1$) extends to a part of $d_2 > 0$ region for $d_1 > 0$. This indicates that we can achieve stability for the fixed COP that is in front of COM, as long as it is sufficiently offset to the right ($d_1 > 0$). We also notice that around the origin, the gradient of the eigenvalues is greater in the direction of y-axis than x-axis of $\{B\}$. This hints that a small displacement of the fixed COP in d_2 should give us a greater control than that of d_1. We utilize this notion in Sect. 4.

Our long-term goal is to match the LLS to biological or robotic locomotion performance, possibly using the LLS as a plant model for control. Therefore, we examined the equilibrium state values, δ^*, θ^*, and $\dot{\theta}^*$, in Fig. 8, as a recipe for future comparisons to biological and robotic systems. As expected, the two contours $\theta^* = 0$ and $\dot{\theta}^* = 0$ indicate purely oddly symmetric (sinusoidal) and evenly symmetric (cosinusoidal) yaw motions, respectively, and these symmetries only occur on those contours.

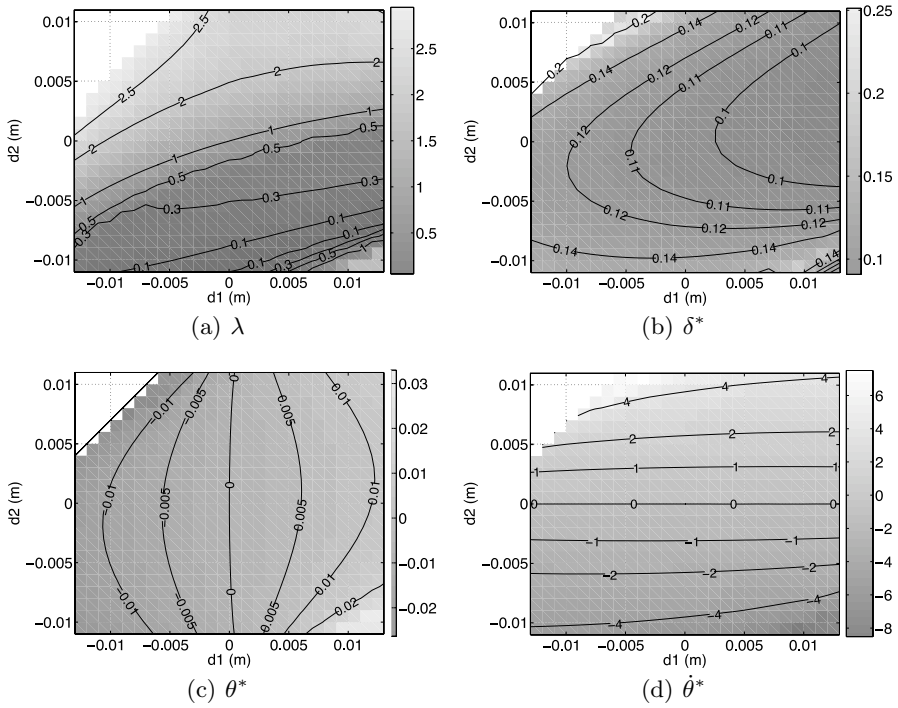

Fig. 8. Contour map of the maximum non-unity eigenvalue and the equilibrium points δ^*, θ^*, and $\dot{\theta}^*$. The parameter values are the same as Fig. 7.

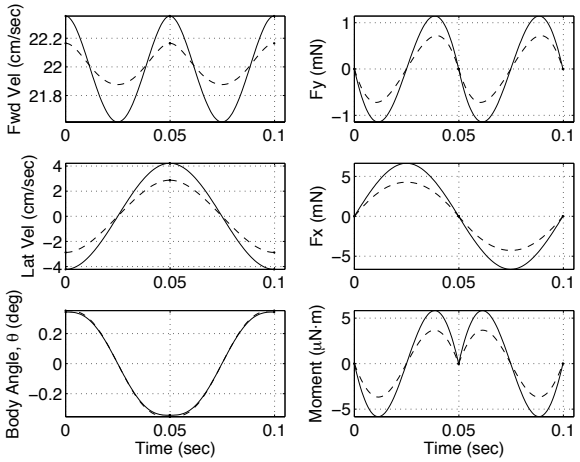

Fig. 9. Comparison between moving and fixed COP. $m = 0.0025\,\mathrm{kg}$, $I = 2.04 \times 10^{-7}\,\mathrm{kg\,m^2}$, $k = 3.52\,\mathrm{N\,m^{-1}}$, $\beta_0 = 1.125\,\mathrm{rad}$. Moving COP (dashed) $v = 0.2235\,\mathrm{m/s}$, $l_0 = 0.0082\,\mathrm{m}$, $d_1 = 0\,\mathrm{m}$, $d_2 = 0.002 \rightarrow -0.002\,\mathrm{m}$. Fixed COP (solid) $v = 0.2275\,\mathrm{m/s}$, $l_0 = 0.0128\,\mathrm{m}$, $d_1 = 0.005\,\mathrm{m}$, $d_2 = 0\,\mathrm{m}$.

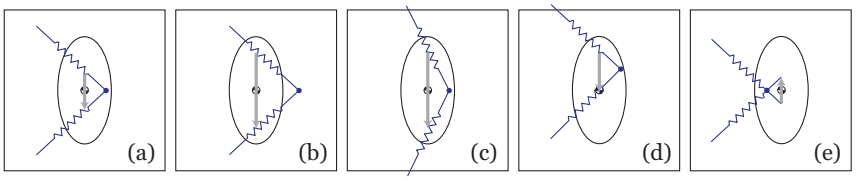

Fig. 10. Comparison between a moving COP and an effective fixed COP during a left step under different protocols. Fixed COP is denoted by a filled dot, and the moving COP is denoted by a gray arrow.

3.3 Comparing Fixed vs. Moving COP Models

From the observations above, we consider the relationship between a fore-aft moving COP and a fixed, laterally offset COP. These two scenarios generate similar waveforms; in fact, using very similar parameters, we can nearly match the body motions and forces using these two strategies, as shown in Fig. 9. To find a good match, we relied on trial and error, using Figs. 4(a) and 5(c) as a guide to adjust d_1 and d_2 and we referred to [22] to adjust l_0, β_0, and k. As shown, the body angle (yaw) motions match nearly exactly, while for the other measurements, the fixed COP exceeded the moving COP somewhat in magnitude, although the results are qualitatively similar.

We compare the moving COP model to a model with a fixed COP on the positive x-axis of $\{B\}$, as follows. As the LLS moves through a left step, the leg intersects the body centerline at a point that moves fore-aft, as depicted in Fig. 10(a). Suppose there is another LLS system with a moving COP that traces out the same path, and has the same foot touchdown position as the fixed COP case. With appropriate parameters (and possibly a nonlinear leg spring), the fixed COP LLS model might approximate the moving COP model. By approximating the moving COP with the fixed COP in this way, we can predict which moving COP protocols might be stable on the basis of the stability contour map (Fig. 7, Sect. 3.2). Using this approach, we address below (without formal proofs) unanswered questions from Sect. 3.1.

In Protocol (c), we considered increasing the magnitude of a moving COP. We approximate this case using the effective fixed COP and effective β_0 shown in Fig. 10(b) and (c); a larger magnitude can be created by moving the effective fixed COP in the x direction and/or decreasing the value of leg touchdown angle β_0. From Fig. 4(a), we saw that the increase in d_1 for a fixed COP improved stability and amplified the body angle and moment, which agrees with increasing the magnitude of fore-aft motion in the moving COP, as shown in Fig. 5(c). Similarly, a moving COP that is shifted forward, as in Protocol (d), can be approximated by shifting the effective fixed COP forward, as shown in Fig. 10(d). Figure 8(a) shows that the effective fixed COP will first be stable, but eventually it will be unstable as the offset increases further.

Earlier, we indicated that the system became unstable when the moving COP moved from back to front (i.e. aft to fore) along the body centerline. As Fig. 10(e) shows, the effective fixed COP would then be placed on the left side of the body centerline which, according to Fig. 8(a), would probably make the system unstable. This also suggests we can achieve stability for a forward moving COP if we choose our offsets carefully.

In Protocol (e), we increased the lateral offset of a moving COP. We can represent this simply by laterally shifting the effective fixed COP which is similar to Protocol (a), Fig. 4(a). Indeed that is what we observed in Fig. 6(e). This explains why the system remained stable when $d_1 < 0$; the effective fixed COP position was to the right of the COM ($d_1 > 0$). This implies that for cockroaches, if their mechanics limit the magnitude of d_2 , i.e. they cannot have a large c_2, then an increase d_1 will achieve the desired stability, or vice versa; this would explain the shift in the moving COP observed in cockroaches [28].

In summary, the moving COP model is more complex than the fixed COP, but they have similar performance in matching biological data. Thus, in the next section, we assume the COP is fixed to the right of the COM within each step, but let the controller adjust the location of the COP between steps.

4 LLS Control: Wall Following

In addition to their remarkable stability, cockroaches also exhibit extraordinary maneuverability. For example the American cockroach, *Periplaneta americana*, follows walls using tactile feedback from their antenna, making up to 25 turns per second in response to jagged walls in the environment [3, 6].

Despite its simplicity, the LLS model captures many salient features of the dynamics and stability of steady-state cockroach locomotion. Building on these strengths, we explored using the LLS as a "plant model" for control. Schmitt and Holmes [24] tested the idea of moving the COP to steer locomotion. They noted that briefly moving the COP in front of the COM generates large turns of 20-70°. Other possible control parameters, such as the spring stiffness, leg length, and step-length can also be used for steering, but Full *et al.* [13] contend that moving the COP is the most effective, and least fragile. Moreover, moving the COP for steering seems to be consistent with animal turning behavior [17].

4.1 LLS Plant Model

In Sect. 3, we compared the effects of moving the COP within a step, versus keeping the COP fixed. Both models can, with appropriate parameters, demonstrate asymptotic stability in the relative heading, δ, and angular velocity, $\dot{\theta}$, but neutral stability in running speed, $v \in \mathbb{R}^+$, orientation θ, and x (if we're running in the y direction of $\{U\}$). As discussed above, the moving COP adds complexity but provides very little advantage over the laterally offset but fixed COP model when it comes to matching steady-state cockroach data. Therefore, we explored using step-to-step adjustments of the COP as an input to control the overall body location in $g \in \mathrm{SE}(2)$. Because there are no energy losses between steps due to impacts, the controlled LLS remains piecewise Hamiltonian and energy conserving.

Initially, we explored control laws that varied d_1, d_2, β_0, and combinations thereof. We found that a highly effective control scheme was to fix β_0 and place the nominal COP to the right of the COM (for left steps), varying only the fore-aft COP location (d_2) from step-to-step. This is consistent with biological observations that rapid maneuvering in cockroaches occurs with large changes in the fore-aft COP [17]. Specifically, we used the step-to-step control input

$$d_k = \alpha e_1 + e_2 u_k, \quad \text{where} \quad e_1 = [\ 1,\ 0\ ]^T,\ e_2 = [\ 0,\ 1\ ]^T, \tag{9}$$

k is the stride number, $u_k \in \mathbb{R}$ is the control input, and α is a scalar. As shown in Sect. 2, selecting $\alpha > 0$ ensures that for $u_k \equiv 0$, the system is asymptotically stable in δ and $\dot{\theta}$, and neutrally stable in v and g. The result is a step-to-step return map,

$$q_{k+1} = f(q_k, u_k), \tag{10}$$

that is no different from the step-to-step uncontrolled LLS in (8), except that between steps the COP location can be adjusted according to (9).

4.2 Antenna-Based Output Function

We assume that the LLS controller will have at its disposal proprioceptive measurements at each step, such as its angular velocity, $\dot{\theta}_k$, and relative heading, δ_k, but not necessarily its position and orientation relative to our arbitrarily assigned world reference frame, $\{U\}$. Therefore, in order for the LLS to achieve some task level goal in SE(2), it needs exteroceptive feedback. For this, we derive inspiration from nature, and assume the LLS has a simplified antenna that measures its distance from a surface in the environment as depicted in Fig. 11.

Our antenna model follows [6–8] and assumes the antenna estimates the distance, γ, from the body centerline to a "wall" – in this case the y-axis – ahead of the COM a known, fixed *preview distance*, ℓ. Under these assumptions

$$\gamma = \ell \tan\theta - x \sec\theta. \tag{11}$$

The above equation (11) relates the LLS pose to the antenna measurement, γ. We make no attempt to avoid collisions of the LLS with the virtual wall and for simplicity, our controller will drive the LLS to align itself directly on top of the y-axis, though this can easily be extended to drive the LLS to follow at an offset distance from the wall. Together, the proprioceptive and exteroceptive measurements yields the measurement function:

$$h(q) := \left[\delta,\ \dot{\theta},\ \gamma\ \right]^T. \tag{12}$$

Fig. 11. *Left:* Multiple exposures of the cockroach *P. americana* negotiating a set of obstacles at high speed, using feedback from its antennae [6]. *Right:* A simplified model of an antenna as a distance-to-wall sensor.

4.3 Reduced Return Map

To simplify controller analysis and design, we reduced the model, by using translational symmetry and energy conservation, as follows. Recall that the left- and right-step mappings, f_L and f_R are invariant to SE(3), but the step-to-step return map, $f = Mf_L$ is not. However, that mapping is invariant to pure y motions (had we chosen a different left-handed frame, translational invariance would have been in the direction of the axis of symmetry of the reflection to that frame). This was by design: our goal for control is wall following, and for simplicity, we have chosen to follow the y-axis. In addition, the output mapping, h, is y-translation invariant. Thus we removed the y equation by setting $y = 0$ at the beginning of each step. Naturally, we ignored the final value of y when finding an equilibrium as we did in Sect. 2. To remove v note that

$$H = \frac{1}{2}mv^2 + \frac{1}{2}I\dot{\theta}^2 + \frac{1}{2}k(\eta - l_0)^2 = H_0 \equiv \text{constant}. \tag{13}$$

So, at each step

$$v = \left[\frac{2}{m}\left(H_0 - \frac{1}{2}I\dot{\theta}^2 - \frac{1}{2}k(\eta - l_0)^2\right)\right]^{1/2}. \tag{14}$$

Thus we defined a transformation

$$T_H : (\delta, \dot{\theta}, \theta, x) \mapsto (v, \delta, \dot{\theta}, \theta, x, 0) \tag{15}$$

that assigns $y = 0$ and computes v from (14). Note that T_H is invertible and T_H^{-1} is the transformation that simply removes the v and y coordinates. Then, we define the reduced variables and mapping

$$q^r = (\delta, \dot{\theta}, \theta, x) \quad \text{and} \quad f^r(q_k^r, u_k) = T_H^{-1}\big(f(T_H(q_k^r), u_k)\big). \tag{16}$$

4.4 Linearized Return Map, Controllability and Observability

As a preliminary control task, we chose to have the LLS follow a virtual "wall" coincident with the y-axis. To find an equilibrium, we used similar techniques to those described in Sect. 2 to find equilibrium trajectories, ensuring that $x = 0$ at the beginning and end of each step, corresponding to exact wall following. The result was an equilibrium q^*, such that $q^* = f^r(q^*, 0)$. To address controllability, we numerically linearized the return map around a nominal equilibrium trajectory, to obtain the local return map

$$\begin{aligned} e_{k+1} &= Ae_k + Bu_k \\ z_k &= Ce_k \end{aligned} \tag{17}$$

where

$$A = \frac{\partial f^r}{\partial q^r}\Big|_{q^r=q^*,u=0} \quad B = \frac{\partial f^r}{\partial u}\Big|_{q^r=q^*,u=0}, \tag{18}$$

and $e_k = q_k^r - q^*$. The linearized output matrix can be derived analytically,

$$C = \left[\frac{\partial h}{\partial q^r}\right]_{q^r=q^*} = \begin{bmatrix} 1 & 0 & 0 & 0 \\ 0 & 1 & 0 & 0 \\ 0 & 0 & \ell & -1 \end{bmatrix} \tag{19}$$

but to date we only have numerical approximations to A and B. The reduced system (A, B, C) is stabilizable and observable for the parameters $m = 0.0025$ kg, $I = 2.04 \times 10^{-7}$ kg m^2, $l_0 = 0.01$ m, $k = 2.25$ N/m, $\beta_0 = 0.8$ rad, and a nominal COP offset of $\alpha = 0.0025$ m.

4.5 Antenna-Based Control Strategy

Because the system is completely observable, state feedback is possible; however, we found that the following simple output feedback to be quite effective:

$$u_k = Kz_k, \tag{20}$$

where z_k is the system output from (17). The closed loop system dynamics are governed by the $e_{k+1} = (A + BKC)e_k$, so to find a good choice for the gain, K, we evaluated the eigenvalues of the system matrix $(A + BKC)$. Amidst a variety of possible feedback gains, we selected $K = [\ 0,\ 0.001,\ 0.1\ ]$, which lead to complex conjugate pairs of closed loop eigenvalues at $-0.4643 \pm j0.2607$ and $0.3478 \pm j0.4827$. A demonstration of this controller, executed on the full nonlinear LLS dynamics, is shown in Fig. 12.

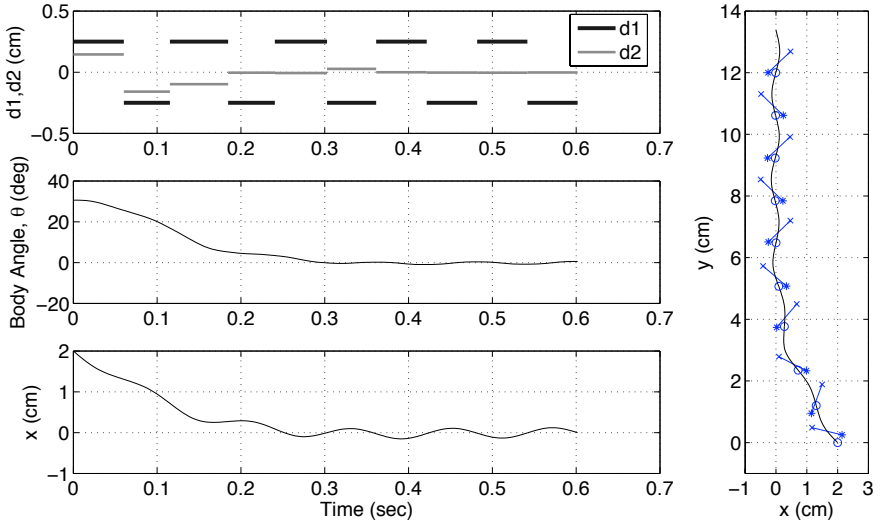

Fig. 12. Simulation of the controlled LLS following the y-axis using the feedback control law (20). In this control law, COP lies nominally along the body x, namely $d = [\ 0.25\text{cm},\ 0\ ]^T$ (for the left step). The output feedback controller (20) varies the COP in the d_2 direction. In the simulation, the LLS starts out rotated 30° counterclockwise from the y-axis, and 2 cm to the right. The figure on the right shows COM ($\circ$), COP ($*$), and foot ($\times$) positions at the start of each step.

5 Conclusion

In this paper, we revised the LLS model to achieve the same phase relationship between the θ and δ as a real cockroach, using a fixed and laterally offset COP. Also we investigated how the COP location governed the overall system stability, and related the fixed COP model to the moving COP model presented by Schmitt and Holmes [23].

For control purposes, we reduced the system state to four dimensions, using translation symmetry and energy conservation. We then applied a very simple output-based feedback strategy to update the COP location between strides based on an antenna-like measurement. Using this controller, the reduced system dynamics were linearly stable. In the future, we will explore using the LLS model as a control template [12] for horizontal-plane control of running robots.

References

1. R. Altendorfer, N. Moore, H. Komsuoglu, M. Buehler, H. B. Brown Jr., D. McMordie, U. Saranli, R. J. Full, and D. E. Koditschek. RHex: A biologically-inspired hexapod runner. *Autonomous Robots*, 11(3):207–213, 2001.
2. R. Blickhan and R. J. Full. Similarity in multilegged locomotion: Bouncing like a monopode. *J Comp Physiol A*, 173:509–517, 1993.
3. J. M. Camhi and E. N. Johnson. High-frequency steering maneuvers mediated by tactile cues: antenna wall-following in the cockroach. *J Exp Bio*, 202:631–643, 1999.
4. G. A. Cavagna, N. C. Heglund, and C. R. Taylor. Walking, running, and galloping: Mechanical similarities between different animals. In T. J. Pedley, editor, *Scale Effects in Animal Locomotion, Proceedings of an International Symposium*, pages 111–125. Academic Press, New York, USA, 1975.
5. J. G. Cham, S. A. Bailey, J. E. Clark, R. J. Full, and M. R. Cutkosky. Fast and robust: Hexapedal robots via shape deposition manufacturing. *The International Journal of Robotics Research*, 21(10), 2002.
6. N. J. Cowan, J. Lee, and R. J. Full. Dynamical control of antennal wall following in the american cockroach. In *The Society for Integrative and Comparative Biology*, page 126, San Diego, CA, January 2005.
7. N. J. Cowan, J. Lee, and R. J. Full. Task-level control of a rapid wall following in the american cockroach. *J Exp Bio*, 2006. In press.
8. N. J. Cowan, E. J. Ma, M. Cutkosky, and R. J. Full. A biologically inspired passive antenna for steering control of a running robot. In *International Symposium on Robotics Research*. Siena, Italy, 2003.
9. M. H. Dickinson, C. T. Farley, R. J. Full, M. R. Koehl, R. Kram, and S. L. Lehman. How animals move: An integrative view. *Science*, 288(5463):100–106, 2000.
10. R. J. Full, R. Blickhan, and L. H. Ting. Leg design in hexapedal runners. *J Exp Biol*, 158:369–390, 1991.
11. R. J. Full and C. T. Farley. Musculoskeletal dynamics in rhythmic systems - A comparative approach to legged locomotion. In J. M. Winters and P. E. Crago, editors, *Biomechanics and Neural Control of Movement*, pages 192–205. Springer-Verlag, New York, 2000.

12. R. J. Full and D. E. Koditschek. Templates and anchors: neuromechanical hypotheses of legged locomotion on land. *J Exp Bio*, 202(23):3325–3332, 1999.
13. R. J. Full, T. M. Kubow, J. Schmitt, P. Holmes, and D. E. Koditschek. Quantifying dynamic stability and maneuverability in legged locomotion. *Integrative and Comparative Biology*, 42(1):149–157, 2002.
14. R. J. Full and M. S. Tu. Mechanics of six-legged runners. *J Exp Bio*, 148:129–146, 1990.
15. R. J. Full and M. S. Tu. Mechanics of a rapid running insect: two-, four-, and six-legged locomotion. *J Exp Bio*, 156:215–231, 1991.
16. F. Iida and R. Pfeifer. "Cheap" rapid locomotion of a quadruped robot: Self-stabilization of bounding gait. In F. Groen, N. Amato, A. Bonarini, E. Yoshida, and B. Krose, editors, *Intelligent Autonomous Systems 8*, pages 642–649. IOS Press, 2004.
17. D. L. Jindrich and R. J. Full. Many-legged maneuverability: Dynamics of turning in hexapods. *J Exp Bio*, 202(12):1603–1623, 1999.
18. R. Kram, B. Wong, and R. J. Full. Three-dimensional kinematics and limb kinetic energy of running cockroaches. *J Exp Bio*, 200:1919–1929, 1997.
19. T. M. Kubow and R. J. Full. The role of the mechanical system in control: a hypothesis of self-stabilization in hexapedal runners. *Philosophical Transactions of the Royal Society of London Serieseoleol B-Biological Sciences*, 354(1385):849–861, 1999.
20. R. D. Quinn, G. M. Nelson, R. J. Bachmann, D. A. Kingsley, J. Offi, and R. E. Ritzmann. Insect designs for improved robot mobility. In Berns and Dillmann, editors, *Conference on Climbing and Walking Robots*, pages 69–76, Karlsruhe, Germany, 2001. Professional Engineering Publications.
21. A. Ruina. Nonholonomic stability aspects of piecewise-holonomic systems. *Rep. Math. Phys.*, 42(1-2):91–100, 1998.
22. J. Schmitt, M. Garcia, R. C. Razo, P. Holmes, and R. J. Full. Dynamics and stability of legged locomotion in the horizontal plane: a test case using insects. *Biol Cybern*, 86:343–353, 2002.
23. J. Schmitt and P. Holmes. Mechanical models for insect locomotion: dynamics and stability in the horizontal plane I. Theory. *Biol Cybern*, 83:501–515, 2000.
24. J. Schmitt and P. Holmes. Mechanical models for insect locomotion: dynamics and stability in the horizontal plane-II. Application. *Biol Cybern*, 83:517–527, 2000.
25. J. Schmitt and P. Holmes. Mechanical models for insect locomotion: active muscles and energy losses. *Biol Cybern*, 89:43–55, 2003.
26. W. J. Schwind and D. E. Koditschek. Approximating the stance map of a 2-dof monoped runner. *Journal of Nonlinear Science*, 10(5):533–568, 2000.
27. A. Seyfarth, H. Geyer, M. Gunther, and R. Blickhan. A movement criterion for running. *J Biomech*, 35(5):649–655, May 2002.
28. L. H. Ting, R. Blickhan, and R. J. Full. Dynamic and static stability in hexapedal runners. *J Exp Biol*, 197:251–269, 1994.